International Letters of Chemistry, Physics and Astronomy
ISSN: 2299-3843, Vol. 72, pp 9-27
doi:10.56431/p-129qm4

Submitted: 2016-07-05
Revised: 2016-09-22
Accepted: 2016-10-03
Online: 2017-01-27

Molecular Structure, Vibrational Spectra and Docking Studies of Abacavir by Density Functional Theory

R. Solaichamy, J. Karpagam*

Department of physics (Engg), Annamalai University, Annamalainagar-608 002, Tamil Nadu, India.

* jkarpagamphd@gmail.com, Mobile: +91 9944721275.

Keywords: Abacavir, FT-IR, FT-Raman, NBO, Molecular Docking, DFT.

Abstract. In this study, optimized geometry, spectroscopic (FT-IR, FT-Raman, UV) analysis, and electronic structure analysis of Abacavir were investigated by utilizing DFT/B3LYP with 6-31G(d,p) as a basis set. Complete vibrational assignments and correlation of the fundamental modes for the title compound were carried out. The calculated molecular geometry has been compared with available X-ray data of Abacavir. The calculated HOMO and LUMO energies show that charge transfer occurs within the molecule. The molecular stability and bond strength have been investigated by applying the Natural Bond Orbital (NBO) analysis. The computational molecular docking studies of title compound have been performed.

1. Introduction

The managing of human immunodeficiency virus (HIV) includes the use of multiple antiretroviral, since single drug therapy becomes ineffective due to development of HIV resistant strains. According to treatment guidelines antiretroviral regimen should contain at least two nucleoside analogue reverse transcriptase inhibitors (NRTIs) and one non-nucleoside reverse transcriptase inhibitor (NNRTI) in a fixed dose combination. This is very efficient in the treatment of HIV. Abacavir (ABC) is a nucleoside reverse transcriptase inhibitor (NRTI) with activity against Human Immunodeficiency Virus Type 1 (HIV-1). ABC is phosphorylated to active metabolites that compete for incorporation into viral DNA. Intracellularly, ABC is converted by cellular enzymes to the active metabolite carbovir triphosphate, an analogue of deoxyguanosine-50-triphosphate (dGTP). Chemically ABC is [(1S,4R)-4-[2-amino-6-(cyclopropylamino)-9H-purin-9-yl] cyclopent-2-en-1-yl] methanol [1,2]. The introduction of highly active antiretroviral therapy (HAART) has profoundly altered both the course and prognosis of HIV infection. After 1996, the availability of protease inhibitors (PI) transformed HIV-infection from a progressive and almost uniformly fatal condition to a treatable chronic infection. Choosing an initial antiretroviral regimen is one of the most important decisions faced by clinicians managing HIV disease. Several antiretroviral combinations have proven sufficiently potent to achieve viral suppression in most treated patients. However, maintaining efficacy depends on other factors, such as the durability of antiviral suppression, tolerability, risk of long-term toxicity, and patient convenience [3].

The present work mainly deals with detailed structural conformation, experimental FT-IR and FT-Raman spectra, vibrational assignments using total energy distribution (TED) and Molecular docking activity as well as DFT/B3LYP calculations for ABC. Vibrational spectra of Abacavir have been analyzed on the basis of calculated total energy distribution (TED). Theoretically computed vibrational wavenumbers were compared with experimental values. The natural bond orbital (NBO) analysis can be employed to identify and substantiate the possible intra and intermolecular interactions between the units that would form the H-bonded network. The UV-Vis spectroscopic studies along with HOMO–LUMO analysis have been used to explain the charge transfer within the molecule.

2. Experimental details

The compound Abacavir was purchased from Aldrich chemicals, USA and used as such to record the FT-IR and FT-Raman, UV spectra. The FT-IR spectrum of Abacavir compound was

recorded in the range of 4000–400 cm^{-1} on a BRUKER Optik GmbH FT-IR spectrometer using KBr pellet technique. The spectrum was recorded in the room temperature, with scanning speed of 10 cm^{-1}, and spectral resolution: 4 cm^{-1}. FT-Raman spectrum of the title compound was recorded using 1064 nm line of Nd:YAG laser as excitation wavelength in the region 3500–50 cm^{-1} on a BRUKER RFS 27: FT-Raman Spectrometer equipped with FT-Raman molecule accessory. The spectral resolution was set to 2 cm^{-1} in back scattering mode. The laser output was kept at 100mW for the solid sample. The ultraviolet absorption spectra of ABC were examined in the range 200–800 nm using Cary 500 UV–VIS–NIR spectrometer. The UV pattern is taken from a 10 to 5 M solution of ABC, dissolved in ethanol solvent. The theoretically predicted IR and Raman spectra at B3LYP/6-31G(d,p) level calculation along with experimental FT-IR and FT-Raman spectra are shown in Fig. 2 and 3.

3. Computational details

The density functional theory DFT/B3LYP with the 6-31G(d,p) as basis set was adopted to calculate the properties of Abacavir in the present work. All the calculations were performed using Gaussian 03W program package [4] with the default convergence criteria without any constraint on the geometry [5]. The assignments of the calculated wavenumbers are aided by the animation option of Gauss View 5.0 graphical interface for Gaussian programs, which gives a visual presentation of the shape of the vibrational modes along with available related molecules [6]. Furthermore, theoretical vibrational spectra of the title compound were interpreted by means of TED using the VEDA 4 program [7]. The optimized structural parameters were used in the vibrational frequency calculations at DFT levels to characterize all stationary points as minima. As the hybrid B3LYP functional tends to overestimate the fundamental normal modes of vibration, the computed frequencies were scaled with appropriate values to bring harmonization between the theoretical and experimental wavenumbers [8]. Vibrational frequencies were computed at DFT level which had reliable one-to-one correspondence with experimental IR and Raman frequencies [9]. The Natural Bond Orbital (NBO) calculations were performed using NBO 3.1 program [10] as implemented in the Gaussian 03W [4] package at the DFT/B3LYP level; in order to understand various second order interactions between filled orbital of one subsystem and vacant orbital of another subsystem which is a measure of the intermolecular delocalization or hyper conjugation.

3.1. Prediction of Raman intensities

The Raman activities (S_{Ra}) calculated with Gaussian 03W program [4] converted to relative Raman intensities (I_{Ra}) using the following relationship derived from the intensity theory of Raman scattering [11]

$$I_i = \frac{f(v_o - v_i)^4 S_i}{v_i[1 - \exp(-hcv_i / kt)]}$$

where, ν_0 is the laser exciting wavenumber in cm^{-1} (in this work, we have used the excitation wavenumber ν_0 = 9398.5 cm^{-1}, which corresponds to the wavelength of 1064 nm of an Nd-YAG laser), ν_i the vibrational wavenumber of the i^{th} normal mode (cm^{-1}) while S_i is the Raman scattering activity of the normal mode ν_i [12].

3.2. Docking Studies

The molecular structure of protein (PDB ID: 3VRI) was taken from RCSB Protein Data Bank, http://www.rcsb.org/pdb [13]. Initial structures of Abacavir were generated by ChemBioOffice 2008. The geometries of Abacavir legand were subsequently optimized at DFT/B3LYP/ 6-31G (d,p) by Gaussian 03 [4]. The molecular modeling docking calculations of Abacavir legand with 3VRI protein were carried out by means of the Autodock tools (ADT) v1.5.4 [14] and Autodock 4.2.3 program from the Scripps Research Institute. In docking study, the search was extended over the whole receptor Abacavir used as blind docking. The grid maps were generated with 0.375 Å spaces using a grid box of 70–70–70 Å. The search was carried out with the

Lamarckian Genetic Algorithm because it has been pointed out to be most efficient, reliable and successful methods in Autodock [15]. The docking parameters used were as follows: GA population size = 150; maximum number of energy evaluation = 25,00,000 and others used were default parameters. The docking conformation with the lowest binding free energy was used for further analysis by Molegro Molecular Viewer software from http:// www.clcbio.com/products/molegro/ [16].

4. Results and Discussions

4.1. Structural analysis

The optimized geometric parameters such as bond lengths, bond angles and dihedral angles of the title molecule were given in Table 1 using DFT calculation with 6-31G(d,p) as a basis set. The atom numbering scheme of the title compound adopted in this study is given in Fig. 1. To the best of our knowledge, experimental data on the geometric structure of the title molecule are not available till date in the literature. Our molecule Abacavir is compared with XRD data of closely related molecules Abacavir methanol 2.5-solvate [17]. The C-C bond length of the purine ring found at C11-C16=1.396 Å and C15-C16=1.414 Å calculated from DFT method which is agree well with XRD value at 1.383 Å and 1.412 Å respectively. The C-N bond length of the purine ring varies from 1.338 Å to 1.335 Å by DFT method 1.334 Å to 1.370 Å by XRD respectively. Similarly, in the cyclopentane ring C-C bond length varies in the range 1.334 Å to 1.556 Å by DFT and 1.329 Å to 1.550 Å by XRD respectively also C-H bond length of this ring found from 1.086 Å to 1.100 Å by DFT and 0.990 Å to 1.000 Å by XRD respectively this is correlate well with calculated values as well as literature data [18]. Methanol group C-H bond lengths are C1-H22=1.102 Å (DFT), 0.990 Å (XRD) and C1-H23=1.095 Å (DFT), 0.990 (XRD). The cyclopropylamine group bond length has been found at C18-C19=1.507 Å (DFT), 1.503 Å (XRD) and C18-C20=1.506 Å (DFT), 1.493 Å (XRD). The N-H bond length of the amino and ammine group is N21-H38=1.008 Å and N21-H39=1.008 Å by DFT method and observed by XRD and N17-H32=1.011 Å (DFT), 0.880 Å (XRD) respectively. The O2-H24 bond length found at 0.965 Å by DFT method and 0.839 Å by XRD.

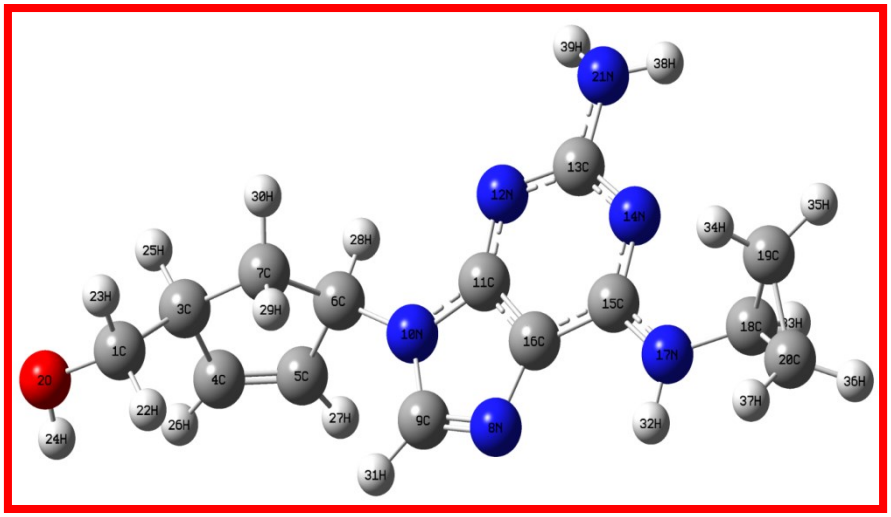

Figure 1. Optimized Molecular structure and atomic numbering of Abacavir.

Table 1. Comparison of experimental and theoretical optimized parameter values of the Abacavir [bond length in (A˚), angles in (◦)].

Bond length	B3LYP	Exp[a]	Bond angle	B3LYP	Exp[a]	Dihedral angle	B3LYP	Exp[a]
C1-O2	1.421	1.419	O2-C1-C3	113.2	111.1	C3-C1-O2-H24	74.28	
C1-C3	1.537	1.526	O2-C1-H22	111.5	109.4	H22-C1-O2-H24	-49.62	
C1-H22	1.102	0.990	O2-C1-H23	105.9	109.4	H23-C1-O2-H24	-165.96	
C1-H23	1.095	0.990	C3-C1-H22	109.4	109.4	O2-C1-C3-C4	-65.38	64.7
O2-H24	0.965	0.839	C3-C1-H23	109.3	109.4	O2-C1-C3-C7	177.31	179.07
C3-C4	1.514	1.495	H22-C1-H23	107.3	108.0	O2-C1-C3-H25	55.35	
C3-C7	1.552	1.554	C1-O2-H24	107.9	109.4	H22-C1-C3-C4	59.63	
C3-H25	1.100	1.000	C1-C3-C4	114.6	109.7	H22-C1-C3-C7	-57.67	
C4-C5	1.334	1.329	C1-C3-C7	113.0	112.7	H22-C1-C3-H25	-179.63	
C4-H26	1.087	0.950	C1-C3-H25	106.7	110.3	H23-C1-C3-C4	176.83	
C5-C6	1.513	1.507	C4-C3-C7	102.8	103.2	H23-C1-C3-C7	59.53	
C5-H27	1.086	0.950	C4-C3-H25	109.0	110.3	H23-C1-C3-H25	-62.43	
C6-C7	1.556	1.550	C7-C3-H25	110.8	110.3	C1-C3-C4-C5	-133.21	
C6-N10	1.462	1.480	C3-C4-C5	112.8	113.6	C1-C3-C4-H26	50.12	
C6-H28	1.096	1.000	C3-C4-H26	122.7	123.2	C7-C3-C4-C5	-10.24	
C7-H29	1.096	0.990	C5-C4-H26	124.3	123.2	C7-C3-C4-H26	173.08	
C7-H30	1.092	0.990	C4-C5-C6	111.8	111.3	H25-C3-C4-C5	107.38	
N8-C9	1.311	1.311	C4-C5-H27	126.2	124.3	H25-C3-C4-H26	-69.30	
N8-C16	1.385	1.393	C6-C5-H27	121.9	124.3	C1-C3-C7-C6	140.65	
C9-N10	1.388	1.374	C5-C6-C7	103.2	104.2	C1-C3-C7-H29	23.72	
C9-H31	1.081	0.950	C5-C6-N10	113.6	111.8	C1-C3-C7-H30	-96.00	
N10-C11	1.380	1.373	C5-C6-H28	110.8	109.2	C4-C3-C7-C6	16.61	
C11-N12	1.339	1.345	C7-C6-N10	114.0	113.3	C4-C3-C7-H29	-100.32	
C11-C16	1.396	1.383	C7-C6-H28	111.0	109.2	C4-C3-C7-H30	139.96	
N12-C13	1.344	1.334	N10-C6-H28	104.4	109.2	H25-C3-C7-C6	-99.75	
C13-N14	1.355	1.370	C3-C7-C6	106.2	105.9	H25-C3-C7-H29	143.32	
C13-N21	1.374	1.355	C3-C7-H29	109.8	110.5	H25-C3-C7-H30	23.60	
N14-C15	1.338	1.347	C3-C7-H30	113.1	110.5	C3-C4-C5-C6	-0.81	
C15-C16	1.414	1.412	C6-C7-H29	108.4	110.5	C3-C4-C5-H27	-177.54	
C15-N17	1.362	1.346	C6-C7-H30	112.1	110.5	H26-C4-C5-C6	175.80	
N17-C18	1.432	1.434	H29-C7-H30	107.3	108.7	H26-C4-C5-H27	-0.93	
N17-H32	1.011	0.880	C9-N8-C16	103.9	-	C4-C5-C6-C7	11.47	
C18-C19	1.507	1.503	N8-C9-N10	113.8	-	C4-C5-C6-N10	135.48	
C18-C20	1.506	1.493	N8-C9-H31	125.3	122.9	C4-C5-C6-H28	-107.38	
C18- H33	1.089	1.000	N10-C9-H31	120.9	122.9	H27-C5-C6-C7	-171.64	
C19-C20	1.509	1.511	C6-N10-C9	128.2	129.2	H27-C5-C6-N10	-47.63	
C19-H34	1.084	0.990	C6-N10-C11	125.9	125.0	H27-C5-C6-H28	69.51	
C19-H35	1.085	0.990	C9-N10-C11	105.9	105.8	C5-C6-C7-C3	-17.12	
C20-H36	1.085	0.990	N10-C11-N12	127.8	-	C5-C6-C7-H29	100.73	
C20-H37	1.086	0.990	N10-C11-C16	105.1	105.6	C5-C6-C7-H30	-141.05	
N21-H38	1.008	0.879	N12-C16-C11	127.1	127.6	N10-C6-C7-C3	-140.86	
N21-H39	1.008	0.880	C11-N12-C13	111.3	111.4	N10-C6-C7-H29	-23.01	
			N12-C13-N14	128.3	127.5	N10-C6-C7-H30	95.21	
			N12-C13-N21	116.5	117.2	H28-C6-C7-C3	101.59	
			N14-C13-N21	115.2	115.2	H28-C6-C7-H29	-140.56	
			C13-N14-C15	118.2	118.7	H28-C6-C7-H30	-22.33	
			N14-C15-C16	119.3	118.5	C5-C6-N10-C9	-44.86	
			N14-C15-N17	120.0	118.9	C5-C6-N10-C11	138.03	146.99
			C16-C15-N17	120.7	122.6	C7-C6-N10-C9	73.04	
			N8-C16-C11	111.4	105.7	C7-C6-N10-C11	-104.07	
			N8-C16-C15	132.9	132.8	H28-C6-N10-C9	-165.68	
			C11-C16-C15	115.7	116.1	H28-C6-N10-C11	17.22	
			C15-N17-C18	123.9	122.4	C16-N8-C9-N10	0.30	
			C15-N17-H32	115.2	118.8	C16-N8-C9-H31	179.60	
			C18-N17-H32	118.6	118.8	C9-N8-C16-C11	-0.25	
			N17-C18-C19	119.2	117.7	C9-N8-C16-C15	-179.16	

			N19-C18-C20	117.3	117.6	N8-C9-N10-C6	-177.81	
			N17-C18-H33	115.3	116.5	N8-C9-N10-C11	-0.25	
			C19-C18-H33	116.6	116.5	H31-C9-N10-C6	2.86	
			C20-C18-H33	117.5	116.5	H31-C9-N10-C11	-179.57	
			C18-C19-H34	116.8	117.8	C6-N10-C11-N12	-2.71	
			C18-C19-H35	117.7	117.8	C6-N10-C11-C16	177.71	179.02
			C20-C19-H34	117.8	117.8	C9-N10-C11-N12	179.65	
			C20-C19-H35	118.8	117.8	C9-N10-C11-C16	0.07	
			H34-C19-H35	114.9	115.0	N10-C11-N12-C13	-179.41	
			C18-C20-H36	117.9	117.8	C16-C11-N12-C13	0.09	
			C18-C20-H37	117.4	117.8	N10-C11-C16-N8	0.11	
			C19-C20-H36	119.0	117.8	N10-C11-C16-C15	179.22	
			C19-C20-H37	117.5	117.8	N12-C11-C16-N8	-179.48	
			H36-C20-H37	114.4	114.9	N12-C11-C16-C15	-0.37	
			C13-N21-H38	115.6	120.0	C11-N12-C13-N14	0.72	
			C13-N21-H39	115.9	120.0	C11-N12-C13-N21	-177.71	
			H38-N21-H39	117.2	120.0	N12-C13-N14-C15	-1.18	
						N21-C13-N14-C15	177.27	
						N12-C13-N21-H38	-162.32	
						N12-C13-N21-H39	-19.49	
						N14-C13-N21-H38	19.05	
						N14-C13-N21-H39	161.87	
						C13-N14-C15-C16	0.76	
						C13-N14-C15-N17	-178.99	
						N14-C15-C16-N8	178.78	
						N14-C15-C16-C11	-0.09	
						N17-C15-C16-N8	-1.47	
						N17-C15-C16-C11	179.66	
						N14-C15-N17-C18	-7.80	
						N14-C15-N17-H32	-170.52	
						C16-C15-N17-C18	172.45	
						C16-C15-N17-H32	9.72	
						C15-N17-C18-C19	82.69	
						C15-N17-C18-C20	151.93	142.2
						C15-N17-C18-H33	-63.34	
						H32-N17-C18-C19	-115.13	
						H32-N17-C18-C20	-45.89	
						H32-N17-C18-H33	98.84	
						N17-C18-C19-H34	-1.64	
						N17-C18-C19-H35	-144.50	
						H33-C18-C19-H34	143.95	
						H33-C18-C19-H35	1.09	
						N17-C18-C20-H36	141.20	
						N17-C18-C20-H37	-2.09	
						H33-C18-C20-H36	-2.75	
						H33-C18-C20-H37	-146.04	
						H34-C19-C20-H36	-146.28	
						H34-C19-C20-H37	-0.91	
						H35-C19-C20-H36	0.18	
						H35-C19-C20-H37	145.55	

N-C-N bond angle for purine ring observed at 113.9° [19]. The purine ring bond angle N12-C13-N14=128.3° by DFT, 127.5° by XRD, this bond angle is good agreement with literature value [19]. The bond angle of cyclopendane ring has been calculated at C4-C3-C7=102.8° by DFT and 103.2° by XRD shows good correlation between calculated and experimental values. The cyclopropyl group C-C-C bond angle has been calculated at N19-C18-C20=117.3°by DFT method. The dihedral angle between purine and cyclopropyl ring has been observed at C15-N17-C18-C20=151.93° (DFT), 142.2° (XRD), similarly dihedral angle between purine and cyclopendane ring is C6-N10-C11-C16=177.71° (DFT), 179.02° (XRD) and C5-C6-N10-C11=138.03°(DFT), 146.99°(DFT) respectively.

4.2. Vibrational assignments

The detailed vibrational assignments (characterized by PED) of fundamental modes of Abacavir along with the calculated IR and Raman intensities are reported in Table 2. Theoretical and corresponding scaled (SQM) frequencies were calculated for title compound at B3LYP/6-31G(d,p) level have been collected along with IR intensities and Raman scattering activities. Theoretically calculated wavenumbers are usually larger than the experimental values, due to the exclusion of scaled frequencies, incomplete incorporation of electron correlation and the use of finite basis set. The over estimations are mostly systematic and can be corrected by following an empirical scaling procedure over the obtained theoretical frequencies fit to the corresponding experimental frequencies. In this study, selective scaling procedures were applied. For the B3LYP/6-31G(d,p) level, the scale factors of 0.9608 reported in reference [20] respectively.

4.2.1. Purine Ring vibrations

The C-C stretching vibrations of the purine ring observed in the Spectral region over 1650–1000 cm^{-1} [21]. In our present investigation C-C stretching vibrations observed at 1606 cm^{-1} in FT-IR and 1607 cm^{-1} in FT-Raman spectrum and calculated at 1595 cm^{-1} and 1569 cm^{-1} by DFT method. The hetero aromatic structure shows the presence of C-H stretching vibrations in the region 3100–3000 cm^{-1}, which is the characteristic region for the ready identification of CH stretching vibrations [22]. For title compound this vibration observed at 3196 cm^{-1} in FT-IR spectrum and 3131 cm^{-1} by DFT method this is a pure mode, the contribution of PED for this mode is 100%. Silverstein et al. [23] assigned C-N, C=N stretching absorption in the region 1382–1266 cm^{-1} for aromatic amines. In our work the purine ring C-N stretching vibration observed at 1500 cm^{-1} in FT-IR spectrum and 1500, 1307 and 1168 cm^{-1} in FT-Raman spectrum. The theoretically predicted wave numbers at 1585, 1499, 1471, 1419, 1370, 1292 and 1289 cm^{-1} by DFT method gives the C-N stretching vibrations. The N-C-N and C-C-N inplane bending vibrations of the purine ring observed at 828 cm^{-1} in IR spectrum and 362 cm^{-1} in FT-Raman spectrum, the calculated wavenumbers at 1005, 824, 364 cm^{-1} and 726, 433, 427 cm^{-1} by DFT method gives the N-C-N and C-C-N inplane bending vibrations respectively. Mode no's 107 and 109 gives the CCCN out of plane bending vibration of the purine ring.

4.2.2. Amino group vibration

According to Socrates [23] the stretching of amino group appeared around 3500–3000 cm^{-1} in absorption spectra. For title molecule the wavenumbers 3465 cm^{-1} and 3592 cm^{-1} calculated by DFT calculations gives the N-H symmetric and antisymmetric stretching vibrations, no bands observed in FT-IR and FT-Raman spectrums for this vibration. The wavenumber at 1569 cm^{-1} predicted by DFT method has been identified as NH_2 scissoring vibration.

4.2.3. Cyclopentane ring vibrations

The C-C stretching vibration of the cyclopentane ring has been computed the scaled wavenumbers at 1029, 904, 812 cm^{-1} by DFT method. The FT-IR band at 750, 564 cm^{-1} and FT-Raman band at 565 cm^{-1} are identified as C-C-C inplane bending vibrations of the cyclopentane ring. C-C-C-C out-of plane bending vibrations observed at 442, 324 cm^{-1} by DFT method and 321 cm^{-1} in FT-Raman band. The C-H stretching vibrations of the cyclopentane ring observed at 2967 cm^{-1} in FT-IR spectrum and 2904 cm^{-1} in FT-Raman spectrum. The computed wavenumbers at 3090, 3062, 3003, 2944 and 2905 cm^{-1} by DFT method gives the C-C stretching vibrations. The CH inplane bending vibrations have been identified at 1258, 1098 cm^{-1} in FT-IR and 1250, 1096 cm^{-1} in FT-Raman spectrum. The mode no's 40, 41, 47, 50 and 51 have been identified as CH inplane bending vibrations. The computed wavenumbers at 1029, 904, 763 and 753 cm^{-1} gives the CCCH torsional vibrations respectively.

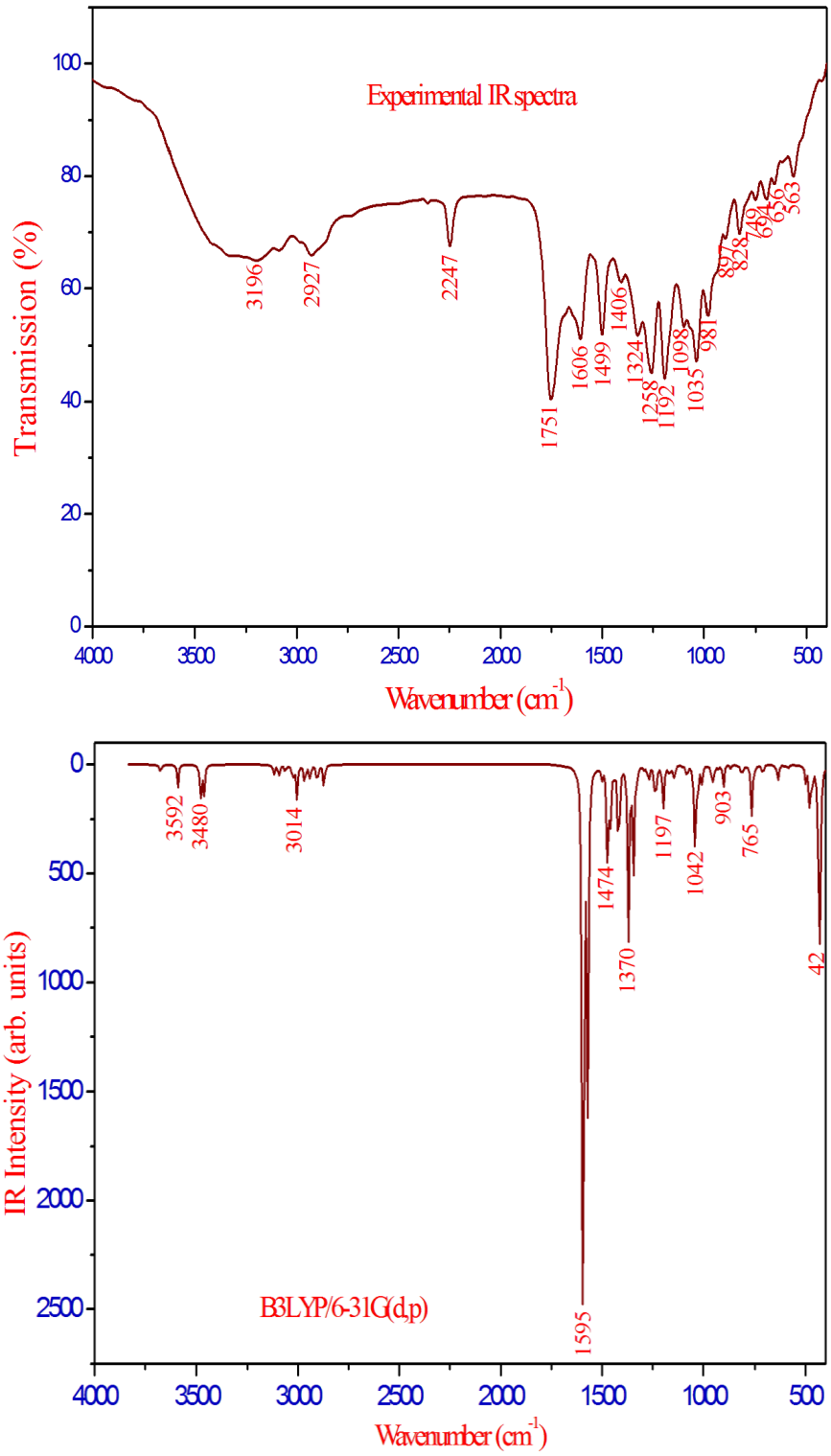

Figure 2. Comparison of experimental and theoretical B3LYP/6-31G(d,p) FT-IR spectrum for Abacavir.

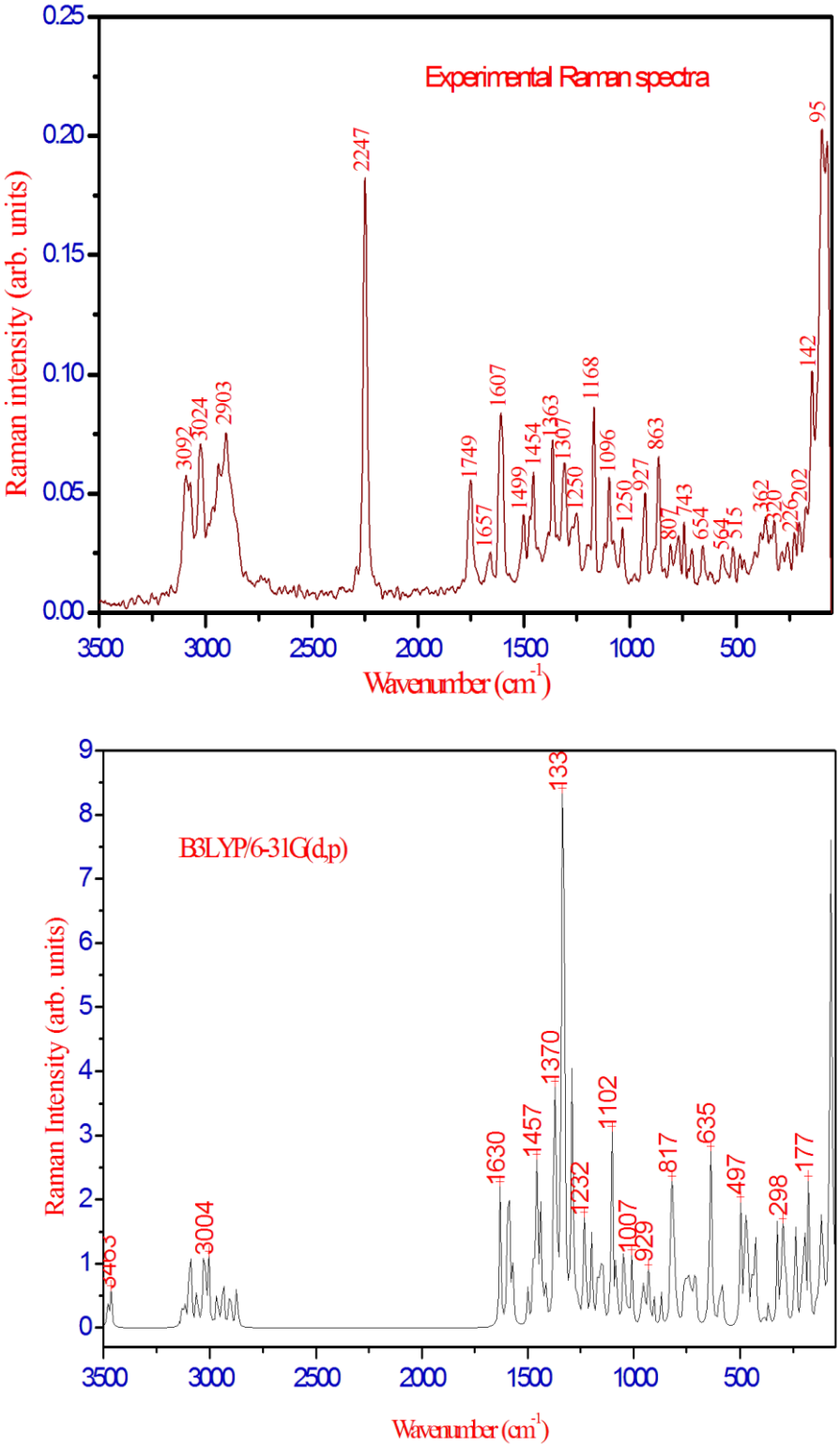

Figure 3. Comparison of experimental and theoretical B3LYP/6-31G(d,p) FT-Raman spectrum for Abacavir.

Table 2. Comparison of the experimental and calculated vibrational spectra and proposed assignments of Abacavir.

Mode No	Experimental wave numbers/cm^{-1}		Theoretical wave numbers/cm^{-1}				Vibrational assignments with PED (≥10%)
	FT-IR	FT-Raman	B3LYP/6-31G(d,p)				
			Unscaled	scaled	I_{IR}[a]	I_{Ra}[b]	
1			3825	3676	13.49	1.89	ν_{O2H24}
2			3739	3592	30.52	2.39	$\nu_{asymN21H38(100)}$
3			3623	3481	44.19	2.94	$\nu_{N17H32(100)}$
4			3606	3465	53.57	7.21	$\nu_{symN21H38(100)}$
5	3196		3259	3131	0.28	3.54	$\nu_{C9H31(100)}$
6			3246	3119	16.21	2.93	$\nu_{asymC19H34(88)}$
7			3226	3100	5.96	4.98	$\nu_{asymC20H36(89)}$
8		3092	3216	3090	13.14	7.31	$\nu_{C5H27(79)}$
9			3187	3062	11.03	6.17	$\nu_{C4H26(80)}$
10			3156	3032	8.44	8.06	$\nu_{symC19H34(95)}$
11		3024	3143	3020	15.78	6.96	$\nu_{symC20H36(95)}$
12			3128	3005	31.06	5.68	$\nu_{C18H33(98)}$
13			3126	3003	17.67	3.21	$\nu_{C7H30(84)}$
14			3088	2967	34.12	5.77	$\nu_{asymC1H23(93)}$
15			3064	2944	14.43	2.01	$\nu_{C6H28(77)}$
16	2927		3057	2937	8.39	5.19	$\nu_{C7H29(69)}$
17		2904	3024	2905	33.13	6.56	$\nu_{C3H25(94)}$
18			2990	2872	36.85	5.66	$\nu_{symC1H22(91)}$
19		1658	1697	1631	1.45	12.73	$\nu_{C4C5(75)}$
20	1606	1607	1660	1595	669.36	8.20	$\nu_{C15C16(20)}+\delta_{H32N17C15(14)}$
21			1649	1585	305.64	10.16	$\nu_{N12C11(24)}+\delta_{C16C11N10(24)}$
22			1633	1569	440.85	4.40	$\delta_{H38N21H39(46)}+ \nu_{C11C16(30)}$
23	1500	1500	1560	1499	15.15	2.98	$\nu_{N8C9(44)}+\delta_{H31C9N8(11)}$
24			1531	1471	180.90	6.29	$\nu_{N8C9(56)}$
25		1455	1518	1459	2.74	3.30	$\delta_{sciH22C1H23(77)}+\tau_{H22C1C3C7(13)}$
26			1517	1458	76.64	10.98	$\tau_{H22C1C3C7(13)}$
27			1504	1445	3.89	2.76	$\delta_{H29C7H30(89)}$
28			1496	1437	8.79	10.57	$\nu_{N12C11(11)}+\delta_{C11C16N8(14)}$
29			1477	1419	104.66	0.63	$\nu_{N12C11(27)}+\delta_{H32N17C15(18)}+ \delta_{sciH36C20H37(51)}$
30	1407		1473	1415	54.46	3.07	$\delta_{sciH34C19H35(71)}$
31			1434	1378	3.23	7.11	$\delta_{H28C6N10(45)}$
32			1426	1370	222.36	15.37	$\nu_{N10C11(21)}+\delta_{H28C6N10(10)}$
33		1363	1419	1364	23.49	3.78	$\delta_{wagH22C1H23(12)}+\gamma_{H22C1C3C7(47)}$
34			1401	1346	155.76	1.15	$\delta_{H33C18N17(44)}$
35			1397	1343	9.86	8.42	$\delta_{H22C1O2(46)}$
36			1392	1337	6.46	12.73	$\delta_{H26C4C5(35)}$
37	1325		1385	1331	31.90	64.03	$\nu_{C15C16(10)}$
38		1307	1345	1292	3.71	9.66	$\nu_{N8C16(22)}$
39			1341	1289	1.85	17.25	$\nu_{N8C16(11)}+\delta_{H25C3C4(19)}+\gamma_{C6C5N10H28(12)}$
40			1322	1270	30.28	1.65	$\delta_{H25C3C4(42)}$
41	1258	1250	1313	1261	1.98	1.27	$\delta_{H26C4C5(13)}+\gamma_{C6C5N10H28(49)}$
42			1288	1238	44.56	2.60	$\tau_{H25C3C4C5(37)}$
43			1279	1229	25.37	10.75	$\nu_{N17C18(10)}+\tau_{H25C3C4C5(17)}$
44	1192		1248	1199	63.94	7.43	$\nu_{C18C19(11)}+\delta_{H33C18N17(16)}$
45			1235	1187	9.53	0.61	$\delta_{H31C9N8(49)}$
46		1168	1218	1170	8.11	3.05	$\nu_{N10C9(50)}$
47			1207	1160	8.58	3.07	$\delta_{H25C3C4(21)}$
48			1199	1152	0.22	2.73	$\delta_{H34C19C20(51)}+\gamma_{H34C19C20C18(15)}$
49			1197	1150	2.66	1.45	$\delta_{H34C19C20(32)}$
50			1189	1143	21.32	4.13	$\delta_{H25C3C4(13)}$
51	1098	1096	1148	1103	1.44	15.79	$\delta_{H26C4C5(69)}$
52			1130	1085	9.21	3.21	$\delta_{H32N21C13(12)}$
53			1126	1082	1.74	1.33	$\tau_{H33C18N17C15(65)}$
54			1119	1075	5.90	1.02	$\nu_{C1C3(20)}$

55			1093	1050	16.61	4.49	$\nu_{N12C13(23)}+\delta_{H38N21C13(28)}$
56			1083	1041	105.37	3.28	$\nu_{O2C1(65)}$
57	1036	1034	1079	1036	2.60	0.49	$\tau_{H36C20C19C18(80)}$
58			1071	1029	49.38	0.74	$\nu_{C3C7(17)}+\delta_{H24O2C1(12)}+\tau_{H22C1C3C7(13)}$
59			1063	1022	5.09	0.64	$\nu_{N14C15(17)}+\tau_{H34C19C20C18(64)}$
60			1049	1008	18.18	3.56	$\nu_{C5C6(19)}+\delta_{C5C6N10(10)}+\gamma_{C7C3C6H29(14)}$
61			1046	1005	7.19	2.35	$\nu_{N12C13(10)}+\delta_{N8C9N10(10)}+\tau_{H34C19C20C18(13)}$
62	981		1005	966	8.73	1.68	$\nu_{C3C7(23)}$
63			992	953	29.08	3.58	$\nu_{C19C20(19)}+\tau_{H34C19C20C18(18)}$
64			980	942	1.54	1.47	$\tau_{H26C4C5H27(83)}$
65		927	965	927	4.89	4.73	$\nu_{C18C20(31)}+\tau_{H33C18N17C15(12)}$
66	897		941	904	31.44	2.08	$\nu_{C5C6(12)}+\tau_{H22C1C3C7(31)}$
67		863	904	869	4.21	2.25	$\nu_{C6C7(12)}+\tau_{H22C1C3C7(15)}+\gamma_{C7C3C6H29(21)}$
68	828		858	824	1.12	5.78	$\nu_{C18C19(11)}+\delta_{N12C13N14(13)}$
69			849	815	5.49	8.00	$\nu_{C18C19(27)}$
70			845	812	9.05	3.22	$\nu_{C6C7(27)}$
71		807	838	805	4.86	4.97	$\nu_{C19C20(19)}+\tau_{H33C18N17C15(45)}$
72			826	793	1.04	0.51	$\tau_{H31C9N8C16(80)}$
73		769	797	765	33.96	1.07	$\tau_{C11N10C9N8(15)}+\gamma_{N21N12N14C13(12)}$
74			794	763	42.92	1.31	$\tau_{H26C4C5C6(15)}$
75	750		783	753	11.42	4.19	$\delta_{C4C5C6(21)}+\tau_{H26C4C5C6(40)}$
76		743	772	742	0.94	4.23	$\delta_{H34C19C20(79)}$
77			756	726	1.07	3.90	$\delta_{C11C16N8(11)}$
78			741	712	5.59	2.06	$\delta_{C3C4C5(15)}+\tau_{C11N10C9N8(13)}+\gamma_{N21N12N14C13(25)}$
79	695	707	736	707	7.93	3.62	$\delta_{C3C4C5(14)}+\tau_{C11N10C9N8(12)}+\gamma_{N21N12N14C13(26)}$
80	656	655	681	654	0.25	0.27	$\gamma_{N12C16N10C11(75)}$
81			664	638	17.13	14.77	$\delta_{N10C11N12(19)}$
82			658	632	13.60	2.05	$\tau_{C11N10C9N8(69)}$
83			620	596	3.64	3.42	$\delta_{N12C13N14(24)}$
84	564	565	607	583	3.79	2.33	$\delta_{C4C5C6(13)}$
85		515	518	497	21.82	7.91	$\delta_{C11N12C13(25)}+\tau_{H32N17C15C16(10)}$
86		483	496	477	82.13	6.22	$\tau_{H32N17C15C16(73)}$
87			488	469	8.87	4.91	$\delta_{C1C3C4(14)}+\tau_{C4C5C6N10(24)}$
88			481	463	14.91	3.36	$\tau_{H38N21C13N14(73)}$
89			460	442	18.40	4.53	$\gamma_{C3C4C5C6(11)}$
90			451	433	105.83	1.13	$\delta_{C19C18N17(22)}+\tau_{H38N21C13N14(20)}$
91			444	427	205.32	4.76	$\delta_{C19C18N17(14)}+\tau_{H38N21C13N14(52)}$
92			404	388	9.72	0.83	$\delta_{C3C1O2(15)}$
93		362	379	364	16.42	2.02	$\delta_{N12C13N21(27)}+\gamma_{C1C4C7C3(12)}$
94		321	337	324	11.93	6.09	$\gamma_{C1C4C7C3(37)}$
95			314	302	5.95	4.85	$\delta_{N12C13N21(11)}+\gamma_{C1C4C7C3(31)}$
96			307	295	103.11	6.48	$\gamma_{H24O2C1C3(70)}$
97			295	284	29.92	3.63	$\tau_{H24O2C1C3(16)}+\gamma_{C1C4C7C3(16)}$
98		258	250	240	5.14	8.17	$\nu_{C15C16}+\delta_{C15N17C18(12)}$
99		226	234	225	1.65	0.16	$\tau_{C13N12C11N10(67)}$
100			219	210	1.65	1.41	$\delta_{C1C3C4(44)}+\tau_{C4C5C6N10(11)}$
101		203	206	198	0.34	9.22	$\delta_{C5C6N10(13)}$
102			182	175	3.03	10.31	$\tau_{C11N12C13N14(26)}$
103		143	144	138	2.97	2.25	$\tau_{C11N12C13N14(51)}$
104			124	119	0.46	8.36	$\delta_{C6N10C9(23)}$
105			110	105	3.83	4.04	$\tau_{C4C3C1O2(41)}$
106		96	85	82	2.20	5.32	$\delta_{N14C15N17(18)}$
107		72	74	71	2.01	35.18	$\gamma_{C6C9C11N10(55)}$
108			46	44	0.55	12.05	$\tau_{C15N17C18C19(69)}$
109			37	35	0.52	6.52	$\gamma_{C6C9C11N10(46)}$
110			24	23	0.15	54.09	$\tau_{C4C5C6N10(52)}+\gamma_{C6C9C11N10(12)}$
111			18	18	0.07	100.00	$\gamma_{C6C9C11N10(80)}$

ν-stretching; δ-in-plane-bending; γ-out-of-plane bending; τ-torsion; w-weak; s-strong; vs-very strong; vw-very weak; m-medium.

[a]I_{IR}-IR Intensity (Kmmol^{-1}); [b]I_{Ra}-Raman intensity (Arb units) (intensity normalized to 100%)

4.2.4. Methylene and OH group vibrations

The asymmetrical stretching (asymCH_2) and symmetrical stretching (symCH_2) bands of the methylene group occur near 2926 and 2853 cm^{-1}, respectively [24]. In our present work the predicted wave numbers at 2967 cm^{-1} and 2872 cm^{-1} are identified as asymmetrical and symmetrical stretching vibrations respectively. The FT-Raman band 1455, 1369 cm^{-1} are observed scissoring and wagging modes of the CH_2 group. These modes are computed at 1459 and 1364 cm^{-1} by DFT method. The O–H stretching vibration is theoretically predicted at 3676 cm^{-1} (mode no. 1) by B3LYP method. The computed wavenumbers at 1343 cm^{-1} and 295 cm^{-1} gives the COH inplane and CCOH out-off plane bending vibrations respectively.

4.2.5. Cyclopropyl ring vibrations

The CH_2 symmetrical and asymmetrical stretching vibrations observed at 3032-3005 cm^{-1} and 3119-3100 cm^{-1} by DFT method. The FT-IR band at 1407 cm^{-1} and computed wavenumbers at 1419, 1415 cm^{-1} by DFT method are identified as scissoring CH_2 vibrations of the Cyclopropyl ring. The C-C stretching vibrations of this ring has been identified at 1192 cm^{-1} in FT-IR and 1199, 815, 805 cm^{-1} by DFT calculation. The C-C-H inplane bending vibrations identified at 1152, 1150, 742 cm^{-1} by DFT method.

4.3. NBO analysis

In the NBO analysis, the electron wave functions are interpreted in terms of a set of occupied Lewis type (bond or lone pair) and a set of unoccupied non-Lewis (anti-bond or Rydberg) localized NBO orbitals. The delocalization of electron density (ED) between these orbitals corresponds to a stabilizing donor acceptor interaction. A useful aspect of the NBO method is that it gives information about interactions in both filled and virtual orbital spaces, which could enhance the analysis of intra- and intermolecular interactions.

The second-order Fock matrix was carried out to evaluate the donor acceptor interactions in the NBO basis. The interactions result in a loss of occupancy from the localized NBO of the idealized Lewis structure into an empty nonLewis orbital. For each donor (i) and acceptor (j), the stabilization energy $E_{(2)}$ associated with the delocalization i / j is estimated as

$$E_2 = \Delta E_{ij} = q_i \frac{F(i,j)^2}{\varepsilon_j - \varepsilon_i}$$

where q_i is the donor orbital occupancy, ε_i and ε_j are diagonal elements and F(i, j) is the off-diagonal NBO Fock matrix element.

The molecular interaction is formed by the orbital overlap between π(C11-C16) → π*(N8-C9), π*(N12-C13), π*(N14-C15) resulting intra molecular charge transfer with stabilization energy is about 18.07, 8.69, 32.98 kCal/mol. The intramolecular hyper conjugate energy between σ and σ* electrons was found as 5.99, 5.72 kCal/mol due to interactions σ(C18-C20) → σ*(C18-C19), σ*(C19-C20). As can be seen from this Table 3, NBO analysis revealed that the π*(N8-C9) →π*(C11-C16), π*(C11-C16), π*(N12-C13) → π*(C11-C16) and π*(N14-C15) → π*(C11-C16) interactions give a strong stabilization to the system of the title compound by 69.21, 124.25 and 204.67 kCal/mol respectively. The interaction between lone pair n(N21) and the antibonding orbital LP(1)N21→π*(N12-C13) with stabilization energy 42.25 kCal/mol.

Table 3. Second order Perturbation theory analysis of Fock Matrix in NBO basis for Abacavir.

Donor (i)	E_D (i)(e)	Acceptor(j)	E_D (j)(e)	$E^{(2)a}$ KJ mol^{-1}	E(j)-E(i)[b] a.u	F(i,j)[c] a.u
σ(C6-H28)	1.965	σ*(C9-N10)	0.042	5.05	0.95	0.062
σ(N8-C9)	1.984	σ*(C15-C16)	0.041	6.76	1.38	0.087
π(N8-C9)	1.905	π*(C11-C16)	0.463	15.72	0.34	0.072
σ(N8-C16)	1.975	σ*(C9-H31)	0.020	5.55	1.23	0.074
σ(C9-N10)	1.984	σ*(C11-N12)	0.018	5.65	1.33	0.077
σ(C11-C16)	1.969	σ*(C6-N10)	0.044	5.63	1.03	0.068
π(C11-C16)	1.648	π*(N8-C9)	0.335	18.07	0.26	0.061
		π*(N12-C13)	0.463	8.69	0.26	0.044
		π*(N14-C15)	0.466	32.98	0.26	0.086
σ(N12-C13)	1.979	σ*(N10-C11)	0.044	8.27	1.28	0.092
π(N12-C13)	1.772	π*(C11-C16)	0.463	31.52	0.32	0.096
		π*(N14-C15)	0.466	5.53	0.30	0.039
π(N14-C15)	1.763	π*(N12-C13)	0.463	36.88	0.30	0.100
σ(N17-H32)	1.981	σ*(N14-C15)	0.016	5.23	1.19	0.070
σ(C18-C19)	1.956	σ*(C18-C20)	0.028	5.75	0.88	0.064
		σ*(C19-C20)	0.021	5.33	0.88	0.061
σ(C18-C20)	1.957	σ*(C18-C19)	0.039	5.99	0.89	0.065
		σ*(C19-C20)	0.021	5.72	0.88	0.064
σ(C19-C20)	1.963	σ*(C18-C19)	0.039	5.17	0.88	0.060
		σ*(C18-C20)	0.028	5.67	0.87	0.063
LP(2)O2	1.954	σ*(C1-C3)	0.037	8.04	0.67	0.066
LP(1)N8	1.926	σ*(C9-N10)	0.042	9.72	0.80	0.079
		σ*(C11-C16)	0.044	6.84	0.93	0.072
LP(1)N10	1.582	σ*(C6-C7)	0.023	6.73	0.60	0.063
		π*(N8-C9)	0.335	45.23	0.27	0.100
		π*(C11-C6)	0.463	40.85	0.29	0.098
LP(1)N12	1.901	σ*(C11-C16)	0.044	10.67	0.90	0.089
		σ*(C13-N14)	0.036	13.14	0.86	0.096
LP(1)N14	1.900	σ*(N12-C13)	0.036	13.79	0.85	0.098
		σ*(C15-C16)	0.041	10.39	0.88	0.087
LP(1)N17	1.724	π*(N14-C15)	0.466	57.31	0.26	0.116
		σ*(C18-C19)	0.039	5.59	0.60	0.055
		σ*(C18-H33)	0.030	7.62	0.73	0.071
LP(1)N21	1.800	π*(N12-C13)	0.463	42.25	0.28	0.104
π*(N8-C9)	0.335	π*(C11-C16)	0.463	69.21	0.02	0.057
π*(N12-C13)	0.463	π*(C11-C16)	0.463	124.25	0.02	0.071
π*(N14-C15)	0.466	π*(C11-C16)	0.463	204.67	0.02	0.082

E_D -means Electron Density

[a]$E^{(2)}$ - means energy of hyper conjugative interactions

[b]Energy difference between donor and acceptor i and j NBO orbitals

[c]F(i,j) is the Fock matrix element between i and j NBO orbitals

4.4. UV-Visible spectral studies

The highest occupied molecular orbitals (HOMOs) and the lowest-lying unoccupied molecular orbitals (LUMOs) are named as frontier molecular orbitals (FMOs). The FMOs play an important role in the optical and electric properties, as well as in quantum chemistry and UV-VIS spectra [26]. Absorption maxima (*λmax*) (nm) for lower-lying singlet states of the molecule of the molecule have been calculated by TD-DFT/B3LYP method. The computed properties such as

absorption wavelength (λ), excitation energies (E), frontier molecular orbital energies, and oscillator strengths (f) are listed in Table 4. Fig. 4 shows the observed UV-Vis spectra of title compound in ethanol solvent. For TD-DFT calculations, the theoretical absorption band was predicted at 240.18 nm with oscillator strength being 0.0906 in ethanol solvent and at 239.68 nm with oscillating strength 0.0765 in gas phase can easily be seen that this corresponds to the experimental absorption at 240 nm. Fig. 5 (a, b) shows the distributions and energy levels of the HOMOs and LUMOs orbitals computed at the B3LYP/6-31G(d,p) level for Abacavir. The conjugated molecules are described by a small HOMO-LUMO separation which is the consequence of a significant amount of intra molecular charge transfer from electron donor groups to the capable electron acceptor groups through π-conjugated path [27]. The calculated energy values of HOMO and LUMO are -5.1506 eV and -0.1474eV and the frontier orbital energy gap value is - 5.0032 eV for Abacavir.

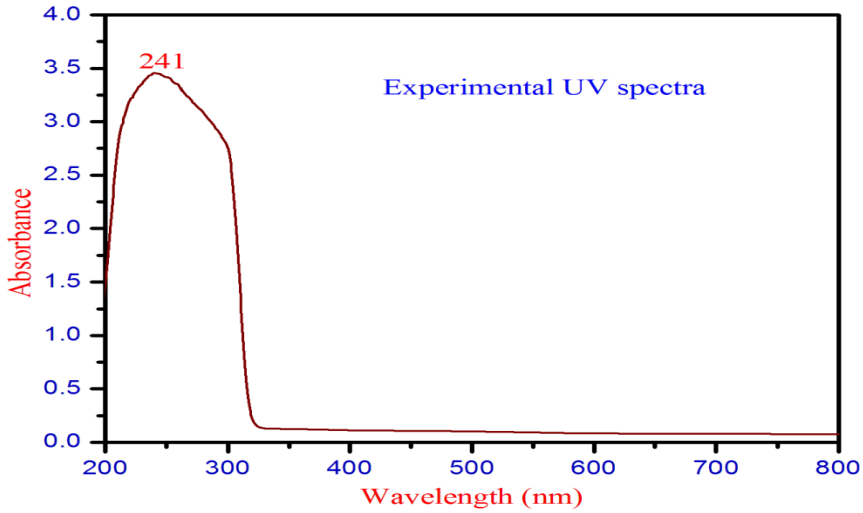

Figure 4. UV-Visible spectrum (Ethanol) of Abacavir.

Table 4. The experimental and computed absorption wavelength λ (nm), excitation energies E (eV), absorbance and oscillator strengths (*f*) of Abacavir in Ethanol solution and gas phase.

Experimental		TD-DFT/B3LYP/6-31G(d,p)					
Ethanol		Ethanol			Gas		
λ(nm)	Abs.	λ(nm)	E(eV)	f(a.u)	λ(nm)	E(eV)	f(a.u)
		266.66	4.6496	0.3502	274.90	4.5101	0.0599
		244.34	5.0743	0.0305	259.43	4.7791	0.2455
240	3.4571	240.18	5.1622	0.0906	239.68	5.1730	0.0765

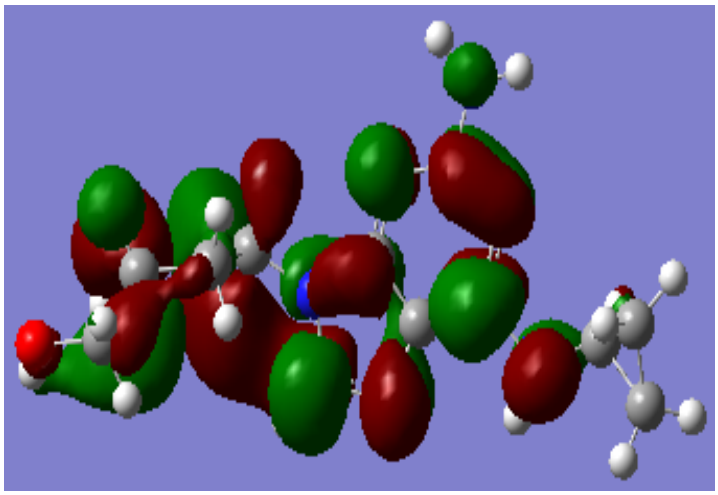

(a) LUMO = -0.1474 eV

Eg = - 5.0032 eV

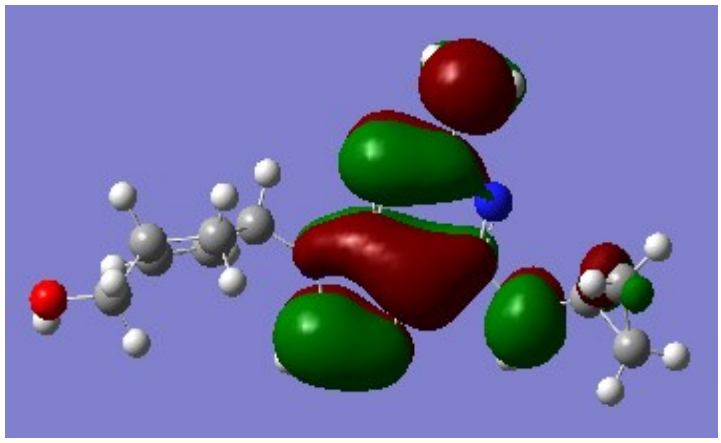

(b) HOMO = -5.1506 eV

Figure 5 (a, b). The atomic orbital compositions of the frontier molecular orbital for Abacavir.

4.5. Molecular electro static potential analysis

MEP is pertained to the electronic density and is a very useful descriptor in understanding sites for nucleophilic reaction and electrophilic attack as well as hydrogen bonding interactions [28]. It also provides visual understanding of relative polarity of the molecule. The MEP surface has been plotted for the molecules Abacavir in Fig. 6. From the Fig.6 it can be seen that region of negative charge is pictured out in red colour and it is found around the electronegative N in the purine ring and O20 atom in the hydroxy groups in the molecule Abacavir. The red region gives the electrophilic attack. The blue colour region represents strong positive region (all hydrogen atoms) and is prone to nucleophilic attack.

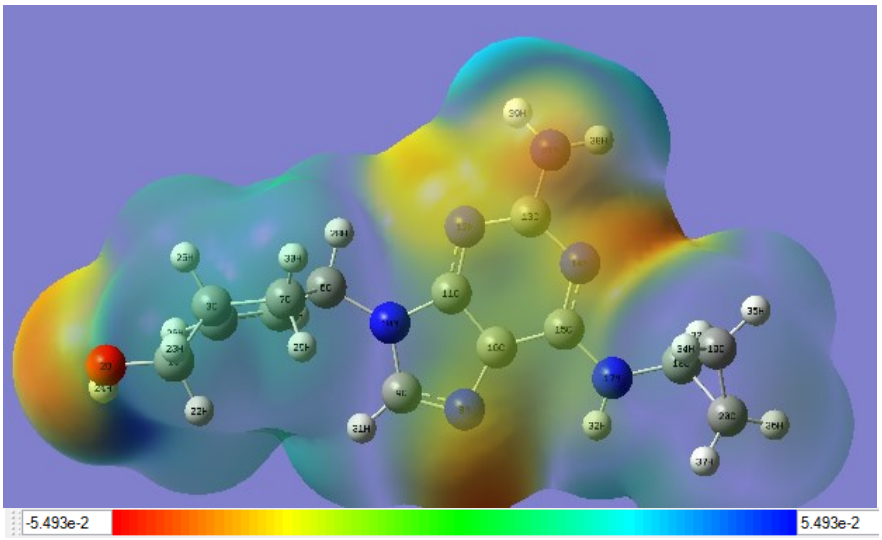

Figure 6. Molecular electro static potential Map of Abacavir.

4.6. Molecular docking studies

Molecular docking studies were performed to investigate the binding affinities of the title compound ABC and the human protein Abacavir, PDB ID: 3VRI [29]. The ligand-protein complex stability was successfully made by some features such as hydrogen bond interactions, vander Waals forces, π-π stacking, hydrophilic and hydrophobic interactions. High resolution crystal structure of Abacavir compound hydrogen and water molecules are reductase was downloaded from the protein data bank website (PDB ID: 3VRI) and all molecular docking calculations were performed on Auto Dock-Vina software [30]. The protein was prepared for docking by removing the co-crystallized ligands, waters and co-factors and the Auto Dock Tools graphical user interface was used to calculate Kollman charges and polar hydrogens. Molecular docking studies were performed to investigate the higher binding affinities and total intermol energy of the newly compound Abacavir is -7.74 kcal/ mol and -5.19 kcal/ mol lower binding affinities and total intermol energy of the title molecules is -9.16 kcal/ mol and -6.62 kcal/ mol respectively. The hydrophobic interactions between ABC and TYR 74, ASP114, Gly-217, SCR116 is found at 2.81 Å, 3.04 Å, and 3.12 Å. On the other hand, a π–π stacking exists between phenyls of ABC and TRP147 is 3.47 Å. The title molecule is given in Fig. 7 and the values are tabulated in Table 5.

Table 5. Comparison of Est. Free Energy of Binding, Total Intermol. Energy of Abacavir.

Mode	Est. Free Energy of Binding	Total Intermol. Energy
1	-7.74 kcal/ mol	-9.16 kcal/ mol
2	-7.39 kcal/ mol	-8.86 kcal/ mol
3	-7.21 kcal/ mol	-8.61 kcal/ mol
4	-5.43 kcal/ mol	-6.79 kcal/ mol
5	-5.19 kcal/ mol	-6.62 kcal/ mol

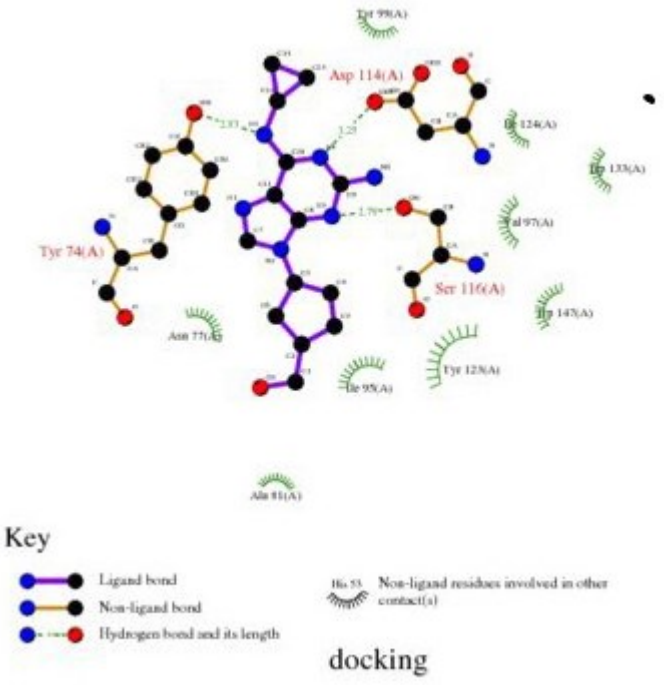

Figure 7a. Hydrogen bonds between docked glutathione and amino acids residues of Abavacir.

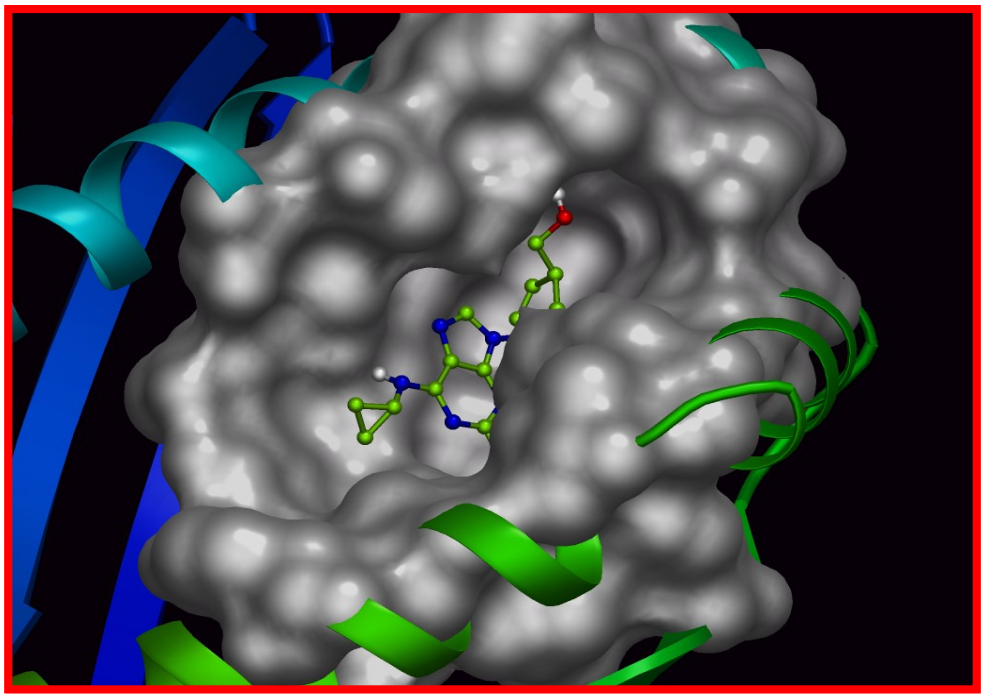

(b)

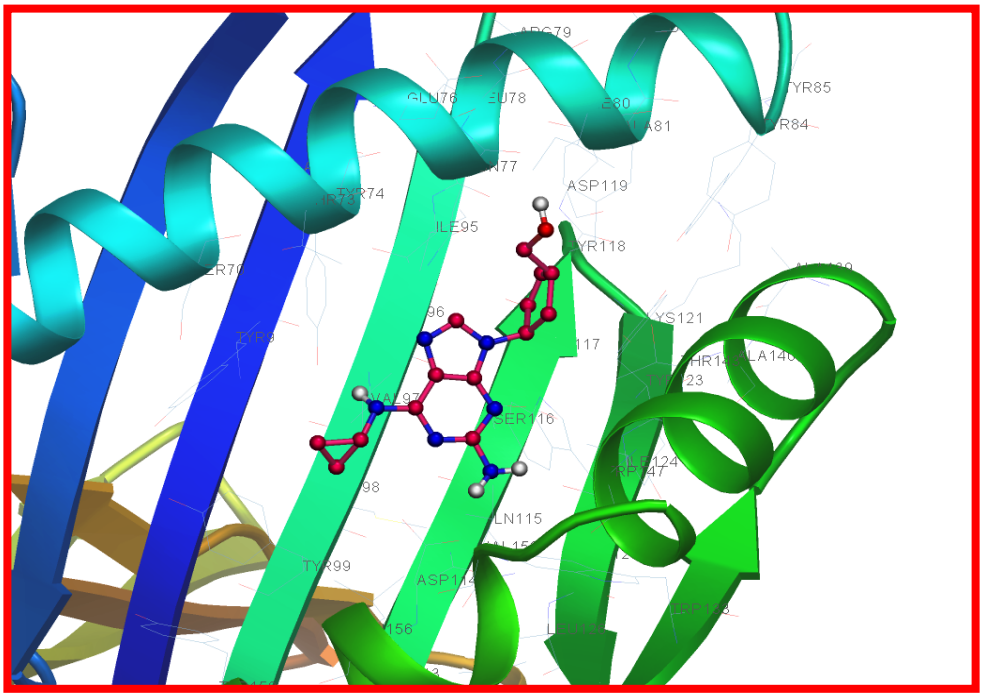

(c)

Figure 7 (b, c). Docked conformation of ligand in the binding site of 3VRI.

5. Conclusions

This paper presents spectroscopic and molecular modeling studies on the interaction of Abacavir using, FT-IR, FT-Raman, UV–Vis spectrum. The equilibrium geometries, HOMO–LUMO analysis and vibrational frequencies of Abacavir have been calculated at B3LYP levels using 6-31G(d,p) basis set. The title molecular HOMO-LUMO energy gap is - 5.0032 eV. The agreement between the optimized and experimental crystal structure is quite good, which shows that the geometry optimization almost exactly reproduces the experimental conformation. The electronic properties are also calculated and compared with the experimental UV–Vis spectrum. The fundamental vibrational modes of the title compound have been precisely assigned and analyzed and the experimental results were compared with the theoretical values. A good agreement between experimental and calculated normal modes of vibrations has been observed. The NBO analysis indicates the intramolecular charge transfer between the bonding and antibonding orbitals. Molecular docking study has been performed by in silico method to analysis their HIVaspects against Abacavir carrier protein. Hydrogen bonds between docked Abacavir and amino acids residues of protein. Docked conformation of ligand in the binding site of Abacavir with 3VRI respectively.

References

[1] P. Kommavarapu et al., Simultaneous estimation of degree of crystallinity in combination drug product of abacavir, lamivudine and neverapine using X-ray powder diffraction technique, Journal of Young Pharmacists. 5(4) (2013) 127–132.

[2] S.K. Gangwer, A.K. Srivastava, R.B. Singh, Experimental [FT-IR, UV-Visible, NMR] spectroscopy and molecular structure, global reactivity parameters, Fukui Function, NBO, NLO, Homo-Lmo, MESP, and QTAM analysei of abacavir using density functional theory, IOSR-journal of Biotechnology and biochemistry. 2 (2016) 19–34.

[3] P. Echeverría, E. Negredo, G. Carosi, Similar antiviral efficacy and tolerability between efavirenz and lopinavir/ritonavir, administered with abacavir/lamivudine (Kivexa), in antiretroviral-naïve patients: A 48-week, multicentre, randomized study (Lake Study), Antiviral Research. 85 (2010) 403–408.

[4] Gaussian Inc., Gaussian 03 Program, Gaussian Inc., Wallingford, 2004.

[5] H.B. Schlegel, Optimization of equilibrium geometries and transition structures, J. Comput. Chem. 3 (1982) 214–218.

[6] A. Frisch, A.B. Nielson, A.J. Holder, Gaussview user manual, Gaussian Inc., Pittsburgh, PA, 2000.

[7] M.H. Jamróz, Vibrational Energy Distribution Analysis, VEDA 4, Warsaw, 2004.

[8] N.C. Handy, P.E. Maslen, R.D. Amos, Study of methane, acetylene, ethene, and benzene using Kohn-Sham theory, J. Phys. Chem. 97 (1993) 4392–4396.

[9] V. Krishnakumar, R. Mathammal, S. Muthunatesan, FT-IR and Raman spectra vibrational assignments and density functional calculations of 1-naphthyl acetic acid, Spectrochim. Acta A. 70 (2008) 210–216.

[10] E.D. Glendening et al., NBO Version3.1, TCI, University of Wisconsin, Madison, 1998.

[11] L. E. Sutton, Tables of interatomic distances, Chemical Society, London, 1958.

[12] K. Govindarasu, E. Kavitha, Vibrational spectra, molecular structure, NBO, NMR, UV, first order hyperpolarizability, analysis of (S)-(−)-N-(5-Nitro-2-pyridyl) alaninol by Density functional theory, Spectrochim. Acta A. 127 (2014) 498–510.

[13] P.T. Illing et al., Immune self-reactivity triggered by drug-modified HLA-peptide repertoire, Nature. 486 (2012) 554-558.

[14] M.F. Sanner, Python: a programming language for software integration and development, Journal of Molecular Graphics and Modelling. 17 (1999) 57–61.

[15] A.A. Adeniyi, P.A. Ajibade, Inhibitory activities and possible anticancer targets of Ru(II)-based complexes using computational docking method, Journal of Molecular Graphics and Modelling. 38 (2012) 60–69.

[16] R. Thomsen, M.H. Christensen, MolDock: A New Technique for High-Accuracy Molecular Docking, J. Med. Chem. 55 (2012) 623-638.

[17] P.TT. Pham, Abacavir methanol 2.5-solvate, Acta Crystallographica Section E: Structure Reports Online. 8 (2009) o193.

[18] A.A. Al-Saadi, J. Laane, Ab initio and DFT calculations for the structure and vibrational spectra of cyclopentene and its isotopomers, J. Mol. Struct. 830 (2007) 46–57.

[19] Ismat Fatima et al., 6-Benzylsulfanyl-9H-purine, Acta Cryst. E. 65 (2009) o2994.

[20] C.S.C. Kumara et al., Synthesis, molecular structure, spectroscopic characterization and quantum chemical calculation studies of (2E)-1-(5-chlorothiophen-2-yl)-3-(2,3,4-trimethoxyphenyl)prop-2-en-1-one, J. Mol. Struct. 1085 (2015) 63–77.

[21] V. Balachandran, K. Parimala, Automeric purine forms of 2-amino-6-chloropurine (N9H10 and N7H10): Structures, vibrational assignments, NBO analysis, hyperpolarizability, HOMO–LUMO study using B3 based density functional calculations, Spectrochimica Acta Part A. 96 (2012) 340–351.

[22] K. Parimala, V. Balachandran, Vibrational spectroscopic (FTIR and FT Raman) studies, first order hyperpolarizabilities and HOMO, LUMO analysis of p-toluenesulfonyl isocyanate using ab initioHF and DFT methods, Spectrochim. Acta A. 81 (2011) 711–723.

[23] M. Silverstein, G.C. Basseler, T.C. Morrill, Spectrometric identification of organic compound, Wiley, New York, 1981.

[24] G. Socrates, Infrared and Raman characteristic group frequencies, Tables and Charts, Third ed., vol. 2, John Wiley, Chichester, 2001.

[25] N.B. Colthup, L.H. Daly, S.E. Wiberley, Introduction to infrared and Raman spectroscopy, Academic Press, New York, 1990.

[26] I. Fleming, Frontier orbitals and organic chemical reactions, Wiley, London, 1976.

[27] C.H. Choi, M. Kertesz, Conformational information from vibrational spectra of styrene, trans-stilbene, and cis-stilbene, J. Phys. Chem. A. 101 (1997) 3823-3831.

[28] N. Okulik, A.H. Jubert, Theoretical analysis of the reactive sites of non–steroidal anti–inflammatory drugs, Internet Electron J. Mol. Des. 4 (2005) 17-30.

[29] N. Strushkevich, S.A. Usanov, H.W. Park, Structural basis of human CYP51 inhibition by antifungal azoles, J. Mol. Biol. 397 (2010) 1067-1078.

[30] O. Trott, A.J. Olson, AutoDock Vina: improving the speed and accuracy of docking with a new scoring function, efficient optimization and multithreading, J. Comput. Chem. 31 (2010) 455-461.